Journal of Solid State Chemistry 183 (2010) 752–759

Contents lists available at ScienceDirect

Journal of Solid State Chemistry

journal homepage: www.elsevier.com/locate/jssc

The $AFeO_2$ (A=K, Rb and Cs) family: A comparative study of structures and structural phase transitions

Naveed Zafar Ali [a], Jürgen Nuss [a], Denis Sheptyakov [b], Martin Jansen [a,*]

[a] Max-Planck-Institut für Festkörperforschung, Heisenbergstraße 1, D-70569 Stuttgart, Germany
[b] Laboratory for Neutron Scattering, ETH Zurich and PSI Villigen, CH-5232 Villigen PSI, Switzerland

ARTICLE INFO

Article history:
Received 28 October 2009
Received in revised form
19 January 2010
Accepted 22 January 2010
Available online 1 February 2010

Keywords:
Azide/nitrate route
Iron
Phase transitions
X-ray diffraction
Synchrotron radiation
Oxoferrates
Cristobalite derivative

ABSTRACT

Structures and phase transitions for the isostructural series of compounds $KFeO_2$, $RbFeO_2$ and $CsFeO_2$ have been systematically studied by synchrotron X-ray high resolution powder diffraction experiments and in case of $CsFeO_2$ also by single crystal diffractometry. At room temperature, all of the three compounds crystallize in the orthorhombic (*Pbca*) $KGaO_2$ type of structure consisting of a three dimensional network of corner-sharing $[FeO_{4/2}]^-$ tetrahedra, which at elevated temperatures shows a reversible phase transformation to a cubic structure (space group $Fd\bar{3}m$). For $KFeO_2$, $RbFeO_2$ and $CsFeO_2$ this phase transformation takes place at 1003 K, 737 K and 350 K respectively, as confirmed by differential scanning calorimetry and X-ray diffraction. Upon heating through the transitions the major structural changes are driven by the onset or enhancement of librational motion of the FeO_4 tetrahedra. Due to this phenomenon the Fe–O–Fe bonds appear to step-wise getting straight, seemingly approaching 180° within the time and space averaged structure.

1. Introduction

The cristobalite type of structure serves as the aristotype for many important synthetic and naturally occurring materials. In particular when including stuffed and substituted structure variants of general formula AMO_2, a vast family of solids is resulting that imposes intriguing challenges for science. Besides the multifaceted phenomena related to cation substitution and ordering on both, the A and M cation sites, the disorder transitions even of the parent cristobalite (SiO_2) continue to attract high interest. The exact nature of the room temperature (α-type) and high temperature (β-cristobalite) form and the microscopic transition mechanism involved has been a subject of great debate in the last decades [1–22].

The structure of α-cristobalite studied earlier by Barth and Nieuwenkamp [1,2] was later well established from single crystal X-ray diffraction studies (tetragonal, $P4_32_12$ or its enantiomorph $P4_12_12$; a=4.98 Å, c=6.95 Å) showing that the crystal structure is a distortional derivative of the high temperature polymorph, β-cristobalite [3,4].

The "ideal" $C9$ type structure (space group $Fd\bar{3}m$) formerly proposed for β-cristobalite by Wyckoff [5] was soon discovered to be physically inconsistent. Barth [6] observed several reflections not allowed by space group $Fd\bar{3}m$, and concluded that the correct space group is $P2_13$. He proposed that the oxygen atoms of the ideal $C9$ structure may either be dynamically disordered and precessing about the [111] direction in an annulus normal to the local Si–O–Si axes. β-cristobalite is now understood to be a time and space averaged structure [7–10].

It has taken many years to achieve a more realistic structure model for β-cristobalite and to better understand the microscopic phenomena involved in the thermally induced reversible displacive structural phase transition ($\alpha \rightarrow \beta$ cristobalite) that can be described via coupled rotations of the MO_4 tetrahedra around mutually orthogonal [110] rotation axes (in such a way that the corner-connected polyhedra remain as close to rigid as possible and/or minimizing the cavities in the tetrahedral framework [11–22]).

In another study the β (low temperature, $Pn2_1a$) to γ (high temperature $P4_12_12$) phase transformation in $NaFeO_2$ has been studied by Rietveld refinement of neutron powder diffraction, showing cooperative rotation of FeO_4 tetrahedra in the cristobalite related $FeO_{4/2}$-framework [23]. Order–disorder phase transitions among different polymorphs of $LiFeO_2$ obtained at different temperature have been systematically studied using X-ray powder diffractometry, neutron diffraction, Moessbauer spectroscopy and transmission electron microscopy [24,25].

Among the most simple stuffed variants of the cristobalite type of structure are the alkali metallates AMO_2, where A represents an alkali metal preferably K, Rb or Cs, while M is a trivalent cation,

* Corresponding author. Fax: +49 711 689 1502.
E-mail address: m.jansen@fkf.mpg.de (M. Jansen).

0022-4596/$ - see front matter © 2010 Elsevier Inc. All rights reserved.
doi:10.1016/j.jssc.2010.01.022

like Al, Ga, Mn, Fe or Co. In these cases the alkali metals enforce a specific tilting pattern of the tetrahedral framework structure, which has been revealed correctly for the first time by Vielhaber and Hoppe [26,27]. For all the representatives known this fully ordered orthorhombic structure is undergoing a structural phase transition to a cubic modification with a dynamically disordered $MO_{4/2}$-framework.

In this report we address the iron based subset $AFeO_2$ with $KFeO_2$ [28], $RbFeO_2$ [29], and $CsFeO_2$ [30]. In retrospective, the first member of the isostructural series, $KFeO_2$, was erroneously reported to have the filled *C*9 structure with space group $Fd\bar{3}m$ ($CsAlO_2$ structure type) with a=7.99 Å [31], but was later known to have a lower symmetry ($KGaO_2$ type) structure [26]. Recently the crystal structure of $RbFeO_2$ was investigated on a six domain twin single crystal and was found to be isostructural to $KGaO_2$ [29], while $CsFeO_2$ was reported to crystallize cubic in the $CsAlO_2$ type of structure [30].

These alkali metal ferrates obviously offer the attractive opportunity for a comparative study of the implications as displayed by stuffed cristobalites. The systematic variation of the size of the respective alkali metal ion, and thus of its ionic strength are expected to determine the static as well as the dynamic tilting of the tetrahedral framework structures, and in particular to affect the Fe–O–Fe bonding angles. We have thus investigated the structural changes with temperatures and the structural phase transitions of $KFeO_2$, $RbFeO_2$, $CsFeO_2$ using X-ray single crystal diffraction, synchrotron powder diffraction and differential scanning calorimetry.

2. Experimental

2.1. Synthesis

All the samples of the isostructural series $AFeO_2$ (A=K, Rb, Cs) were prepared using the "azide nitrate route" [32,33] from KNO_3 (E. Merck, 99%), $RbNO_3$ (E. Merck, 99%) and $CsNO_3$ (Sigma Aldrich, 99%) respectively, the respective alkali metal azide (AN_3) and active iron oxide (Fe_2O_3) according to Eq. (1).

$$5AN_3 + ANO_3 + 3Fe_2O_3 \rightarrow 6AFeO_2 + 8N_2 \ (A\text{=K, Rb and Cs}) \quad (1)$$

The alkali metal azides were synthesized from aqueous HN_3 and alkali metal carbonates [34]. Active iron(III) oxide, Fe_2O_3, was prepared by heating $FeC_2O_4 \cdot 2H_2O$ in a flow of oxygen at 623 K for 20 h. The phase purity of the precursors was monitored by X-ray powder analysis.

The starting materials were mixed in the ratio required according to Eq. (1), ground thoroughly in an agate mortar, pressed into pellets ($\varnothing$ =6 mm) under pressure of 35 kbar, dried in vacuum (10^{-3} mbar) at 400 K for 12 h and placed under argon into a tightly closed steel vessel, provided with a silver inlay [33]. In a flow of dry argon the following temperature profile was applied: 298–533 K (100 K h^{-1}); 533–653 K (5 K h^{-1}); 653 – T_{max} (20 K h^{-1}) with subsequent annealing for 50 h at T_{max}=793 K for $RbFeO_2$, 833 K for $CsFeO_2$ and 873 K for $KFeO_2$. The reaction vessels were cooled down slowly to 673 K (5 K h^{-1}) and then to room temperature at a rate of 100 K h^{-1}. The pure single phase powders obtained are very sensitive to humid air and must be handled in an inert atmosphere.

2.2. X-ray single crystal diffraction

Single crystals of $CsFeO_2$ have been grown by post annealing the reaction product at 773 K for 500 h. For this purpose, the microcrystalline primary product was pressed into pellets and placed in silver crucibles, closed with a silver stopper. The crucibles were sealed in glass ampoules under dried argon. Single crystals of $CsFeO_2$ were selected in a dry box under an argon atmosphere (O_2, H_2O < 0.1 p.p.m., M. Braun GmbH, Garching, Germany) and mounted in a sealed glass capillaries.

Diffraction intensities were collected with a SMART APEX I three-cycle diffractometer (Bruker AXS, Karlsruhe, Germany) with Mo-$K\alpha$ radiation (λ=0.71073 Å) at room temperature (298 K), 100 and 400 K. The 100 and 400 K measurements were performed with a 700^{plus} Cryostream cooler [Oxford Cryosystems Ltd., Oxford, UK (80–500 K)].

The collection and reduction of data were carried out with the *Bruker Suite* software package [35]. A detailed analysis of the collected diffraction intensities at room temperature for all the three ferrates under investigation revealed the same twinning phenomenon as already observed for $RbFeO_2$ [29]. The full pattern can be interpreted as a superposition of six differently oriented but identical diffraction patterns. The handling for data processing of this reticular pseudo-merohedrally twinned crystal is described in detail somewhere else [29,36]. An absorption correction was applied using *TWINABS* [37] for the room temperature and low temperature measurements; and *SADABS* [38] for the high temperature measurement, respectively. Fig. 1 shows the reciprocal layer *hk*0, for the orthorhombic room temperature phase, with pseudo cubic symmetry due to twinning, and the cubic high temperature phase of $CsFeO_2$. The polyhedron represents the six different orientations (six colors) of the six domains with cubic symmetry in total (shape of polyhedron).

The room and high-temperature structures were refined by full-matrix least-squares fitting with the *SHELXTL* software package [39], within the space groups *Pbca* and $Fd\bar{3}m$, whereby the atomic coordinates of $RbFeO_2$ [29] and $CsAlO_2$ [40] were used as starting models for the room temperature and high temperature modifications, respectively. Experimental details on crystallographic data and data collection are given in Table 1, atomic coordinates and isotropic

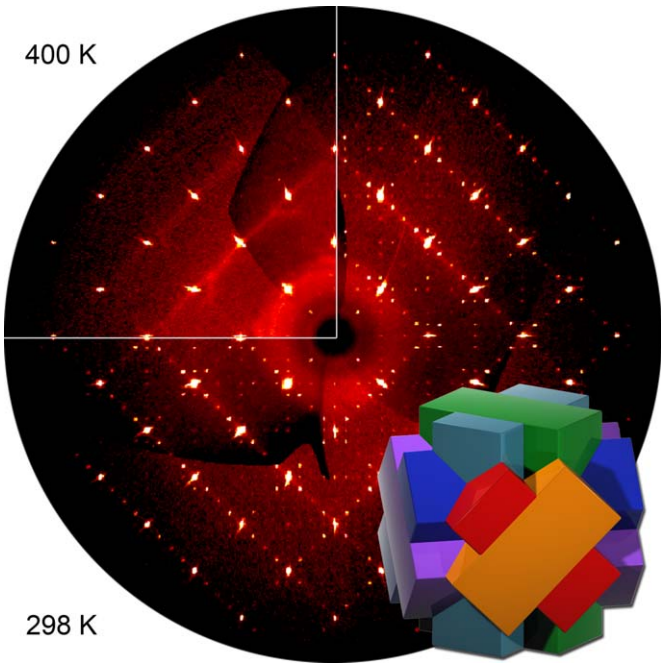

Fig. 1. Reciprocal layer *hk*0 for the orthorhombic room temperature phase, with pseudo cubic symmetry due to twinning, and the cubic high temperature phase of $CsFeO_2$. The polyhedron represents the six different orientations (six colors) of the six domains. Without paying attention to the colors, the polyhedron has the cubic symmetry $m\bar{3}m$, which also corresponds to the Laue group observed in the diffraction pattern.

Table 1
Crystallographic data for $CsFeO_2$ at different temperatures (obtained from single crystal diffraction data).

Temperature/K	100.0(2)	298.0(2)	400.0(2)
Formula weight		220.76	
Crystal system	Orthorhombic	Orthorhombic	Cubic
Space group, Z	*Pbca*, 16	*Pbca*, 16	$Fd\bar{3}m$, 8
Lattice constants/Å	a=5.8876(6)	a=5.9137(6)	a=8.406(1)
	b=11.855(1)	b=11.894(1)	
	c=16.733(2)	c=16.776(2)	
Volume/Å^3	1168.0(2)	1180.0(2)	593.9(1)
Density (calc.)/g cm^{-3}	5.022	4.971	4.938
Diffractometer		SMART APEX I, Bruker AXS	
Radiation type		Mo$K\alpha$, 0.7103 Å	
θ range/°	2.43–35.07	2.43–35.12	4.20–34.56
Absorption correction	Multi-scan (based on symmetry related measurements)		
	TWINABS [37]	TWINABS [37]	SADABS [38]
Reflections collected	12 681	11 953	2102
Independent reflections. R_{int}	–	–	84, 0.037
No. of parameters	79	79	5
$R_1[F^2>2\sigma(F^2)]$, $wR(F^2)$]	0.094, 0.255	0.120, 0.362	0.154, 0.615
Twin volume fractions	0.175(1), 0.242(1), 0.170(1), 0.175(1), 0.117(1), 0.121(1)	0.180(2), 0.238(2), 0.174(2), 0.176(2), 0.117(2), 0.115(2)	–
Deposition no.	CSD-421171	CSD-421172	CSD-421173

Table 2
Atomic coordinates and equivalent isotropic displacement parameters U_{eq}/Å^2 for $CsFeO_2$ at different temperatures (refined from single crystal diffraction data).

Temperature (K)	Atom	Site	x	y	z	U_{eq}
100	Cs1	8*c*	0.75324(6)	0.00477(4)	0.06221(3)	0.0179(1)
	Cs2	8*c*	0.2897(1)	0.25518(3)	0.31295(3)	0.0197(1)
	Fe1	8*c*	0.2502(1)	0.00323(8)	0.18715(6)	0.0070(2)
	Fe2	8*c*	0.7737(2)	0.25474(7)	0.43551(6)	0.0077(2)
	O1	8*c*	0.306(1)	0.1414(5)	0.1373(4)	0.027(1)
	O2	8*c*	0.186(1)	0.1123(5)	0.6143(4)	0.020(1)
	O3	8*c*	0.0520(9)	0.2229(4)	0.9859(3)	0.0177(9)
	O4	8*c*	0.9617(8)	0.9899(4)	0.2323(3)	0.0158(8)
298	Cs1	8*c*	0.75287(9)	0.00263(5)	0.06220(4)	0.0295(2)
	Cs2	8*c*	0.2771(1)	0.25272(5)	0.31305(4)	0.0319(2)
	Fe1	8*c*	0.2501(1)	0.00234(7)	0.18713(6)	0.093(2)
	Fe2	8*c*	0.7681(2)	0.25289(8)	0.43569(6)	0.0093(2)
	O1	8*c*	0.313(2)	0.1383(6)	0.1354(5)	0.047(2)
	O2	8*c*	0.185(1)	0.1199(6)	0.6207(5)	0.040(2)
	O3	8*c*	0.0373(9)	0.2257(5)	0.9908(3)	0.024(1)
	O4	8*c*	0.9723(9)	0.9932(5)	0.2370(4)	0.028(1)
400	Cs	8*b*	3/8	3/8	3/8	0.059(4)
	Fe	8*a*	1/8	1/8	1/8	0.021(3)
	O	16*c*	0	0	0	0.071(9)

displacement parameters are given in Table 2. Further details may be obtained from Fachinformationszentrum Karlsruhe, 76344 Eggenstein-Leopoldshafen, Germany [Fax: (+49)-7247-808-666; E-Mail: crysdata(at)fiz-karlsruhe.de, http://www.fiz-karlsruhe.de/request for deposited data.html] on quoting the CSD-numbers given in Table 1.

2.3. High-resolution synchrotron powder diffraction

The synchrotron X-ray powder diffraction experiments were carried out at the powder diffraction station of the Materials Sciences (MS-Powder) beamline at the Swiss Light Source [SLS], with the use of the Microstrip Detector Mythen-II [41]. The diffraction patterns were collected on heating the powder samples enclosed in the Hilgenberg quartz-glass capillaries with a diameter 0.3 mm in the STOE oven, with an X-ray wavelength of 0.497 Å.

The Synchrotron patterns were measured in the range of T=298–1239 K with steps of 8 K for $KFeO_2$, in the range of T=298–783 K with steps of 5 K for $RbFeO_2$, whereas data collection for $CsFeO_2$ was done in the range of T=298–409 K with steps of 1 K.

For $RbFeO_2$ a partial decomposition, as indicated by the appearance of Fe_3O_4 at temperatures starting from ~680 K, was observed. At the highest temperature assessed for $RbFeO_2$, the weight proportion of this impurity amounted up to ~4% (based on the results of two-phase Rietveld refinements). Upon cooling it remained at exactly this value.

When heating $KFeO_2$, an even more severe decomposition was observed in the X-ray diffraction patterns parallel to the evolution of the crystal structure. The phases emerging at high temperatures included: Fe_3O_4 (starting from ~720 K) [42] and some potassium poor oxoferrates. These were identified as rhombohedral $K_{\sim 0.15}Fe_{10}O_{\sim 15.6}$ [43] (starting from ~900 K), K-deficient cubic phase with a probable composition $K_{\sim 0.67}FeO_2$ and an orthorhombic phase with an approximate composition $K_7Fe_5O_{16}$ [44], (both starting from ~940 K). The origin of partial decomposition of the sample at higher temperature is the reaction of the powder with wall of quartz capillary. No decomposition was observed in case of high temperature neutron scattering experiment where a vanadium container was used [50].

It is grace to the high resolution of the synchrotron diffraction patterns collected which allowed for the phases identification, and for a multi component Rietveld refinement. The collected data were refined using the program Fullprof [45] based on the Rietveld procedure.

Experimental details, crystallographic data, and atomic coordinates are given in Tables 3 and 4. Further details may be obtained from Fachinformationszentrum Karlsruhe, 76344 Eggenstein-Leopoldshafen, Germany [Fax: (+49)-7247-808-666; E-Mail: crysdata(at)fiz-karlsruhe.de, http://www.fiz-karlsruhe.de/request for deposited data.html] on quoting the CSD-numbers given in Table 3.

2.4. Thermal analysis

The differential scanning calorimetry (DSC) measurements were carried out with a DSC device (DSC 404 C, Netzsch GmbH, Selb, Germany). The samples were heated at a rate of 5 K min^{-1} in a corundum crucible under dry argon.

Table 3
Crystallographic data for $AFeO_2$ (A=K, Rb, Cs) at different temperatures (obtained from powder synchrotron data).

Compound	$KFeO_2$		$RbFeO_2$		$CsFeO_2$	
Temperature/K	303	1015	303	783	303	400
Formula weight	126.94		173.32		220.76	
Crystal system	Orthorhombic	Cubic	Orthorhombic	Cubic	Orthorhombic	cubic
Space group, Z	*Pbca*, 16	$Fd\bar{3}m$, 8	*Pbca*, 16	$Fd\bar{3}m$, 8	*Pbca*, 16	$Fd\bar{3}m$, 8
Lattice constants/Å	a=5.59483(1)	a=8.07754(2)	a=5.71547(1)	a=8.227186(6)	a=5.915303(8)	a=8.411704(3)
	b=11.24908(3)		b=11.50563(4)		b=11.88481(2)	
	c=15.93549(4)		c=16.34578(5)		c=16.77518(2)	
Volume/Å^3	1002.926(4)	527.032(2)	1074.899(6)	556.870(1)	1179.333(3)	595.185(1)
ρ (calc.)/g cm^{-3}	3.362	3.200	4.283	4.133	4.972	4.926
Diffractometer	Powder diffraction station of the Materials Science Beamline at the SLS, equipped with the microstrip detector					
Radiation type	Synchrotron, 0.497015 Å					
θ range/°	3.0–54.0	3.0–37.0	3.0–37.3	3.0–37.3	3.0–53.38	3.0–53.38
Data points	13 567	9051	9131	9131	13411	13411
No. of reflections	3195	41	1203	45	3646	114
No. of parameters	75	79	65	43	74	48
R_p, R_{wp}, χ^2	2.927, 3.853, 1.12	3.263, 4.720, 1.75	2.04, 2.65, 1.84	2.03 2.66, 1.74	2.63, 3.34, 1.31	2.743, 3.50, 1.46
Deposition no.	CSD-421185	CSD-421186	CSD-421187	CSD-421188	CSD-421189	CSD-421190

Table 4
Atomic coordinates and equivalent isotropic displacement parameters U_{eq}/Å^2 for $AFeO_2$ (A=K, Rb, Cs) at different temperatures (refined from powder synchrotron data).

Compound, T	Atom	Site	x	y	z	U_{eq}
$KFeO_2$, 298 K	K1	8*c*	0.754(1)	0.0104(5)	0.0652(5)	0.0141(7)
	K2	8*c*	0.3041(7)	0.2611(5)	0.3157(5)	*U*(K1)
	Fe1	8*c*	0.2527(7)	0.0100(4)	0.1897(4)	0.0179(7)
	Fe2	8*c*	0.7858(6)	0.2644(3)	0.4368(4)	*U*(Fe1)
	O1	8*c*	0.298(2)	0.1578(12)	0.1529(7)	0.011(1)
	O2	8*c*	0.173(2)	0.0943(13)	0.6018(8)	*U*(O1)
	O3	8*c*	0.082(2)	0.2042(12)	0.9809(7)	*U*(O1)
	O4	8*c*	0.937(2)	0.9811(12)	0.2152(8)	*U*(O1)
$KFeO_2$, 1015 K	K	8*b*	3/8	3/8	3/8	0.101(1)
	Fe	8*a*	1/8	1/8	1/8	0.0432(5)
	O	16*c*	0	0	0	0.231(3)
$RbFeO_2$, 298 K	Rb1	8*c*	0.754(2)	0.0095(4)	0.0621(5)	0.0245(9)
	Rb2	8*c*	0.3003(6)	0.2595(5)	0.3133(5)	*U*(Rb1)
	Fe1	8*c*	0.258(1)	0.0076(6)	0.1901(6)	0.0047(9)
	Fe2	8*c*	0.7852(8)	0.2598(6)	0.4370(6)	*U*(Fe1)
	O1	8*c*	0.278(3)	0.1521(19)	0.1496(11)	0.010(3)
	O2	8*c*	0.173(3)	0.096(2)	0.6114(14)	*U*(O1)
	O3	8*c*	0.073(3)	0.212(2)	0.9869(10)	*U*(O1)
	O4	8*c*	0.959(3)	0.9796(19)	0.2230(12)	*U*(O1)
$RbFeO_2$, 783 K	Rb	8*b*	3/8	3/8	3/8	0.0701(10)
	Fe	8*a*	1/8	1/8	1/8	0.0653(6)
	O	16*c*	0	0	0	0.150(3)
$CsFeO_2$, 298 K	Cs1	8*c*	0.7503(4)	0.0034(1)	0.0624(2)	0.0236(1)
	Cs2	8*c*	0.2837(1)	0.2532(2)	0.3123(2)	*U*(Cs1)
	Fe1	8*c*	0.2540(7)	0.0031(4)	0.1872(4)	0.0098(2)
	Fe2	8*c*	0.7744(2)	0.2531(4)	0.4381(4)	*U*(Fe1)
	O1	8*c*	0.286(1)	0.140(1)	0.1391(8)	0.0096(9)
	O2	8*c*	0.194(1)	0.116(1)	0.6200(9)	*U*(O1)
	O3	8*c*	0.055(1)	0.2250(9)	0.9857(4)	*U*(O1)
	O4	8*c*	0.974(2)	0.985(1)	0.2334(7)	*U*(O1)
$CsFeO_2$, 400 K	Cs	8*b*	3/8	3/8	3/8	0.0368(1)
	Fe	8*a*	1/8	1/8	1/8	0.0163(1)
	O	16*c*	0	0	0	0.0660(8)

3. Results and discussion

The title compounds $KFeO_2$, $RbFeO_2$, and $CsFeO_2$ were prepared along the azide/nitrate route [32] as olive green, microcrystalline, pure phases in gram amounts. All of those oxoferrates(III) compounds crystallize in the $KGaO_2$ type of structure, at room temperature, which is a displacive, ordered variant of the $CsAlO_2$ type (see Fig. 2).

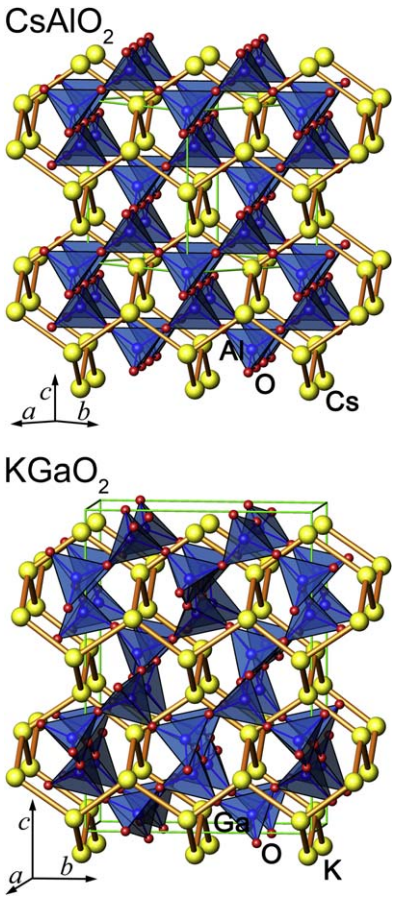

Fig. 2. Crystal structure of cubic $CsAlO_2$ (top) and orthorhombic $KGaO_2$ (below), with unit cells drawn in.

3.1. Structural phase transitions

As known from the past, $KFeO_2$ is undergoing the structural phase transition near its Néel temperature such that "*The structure above T_N should be more regular*" [46].

The thermodynamics of the high temperature transition was investigated using DSC as seen in Fig. 3 on each of these samples, showing transitions to occur at ~988 K in case of $KFeO_2$, ~721 K for $RbFeO_2$, and ~346 K for $CsFeO_2$, respectively.

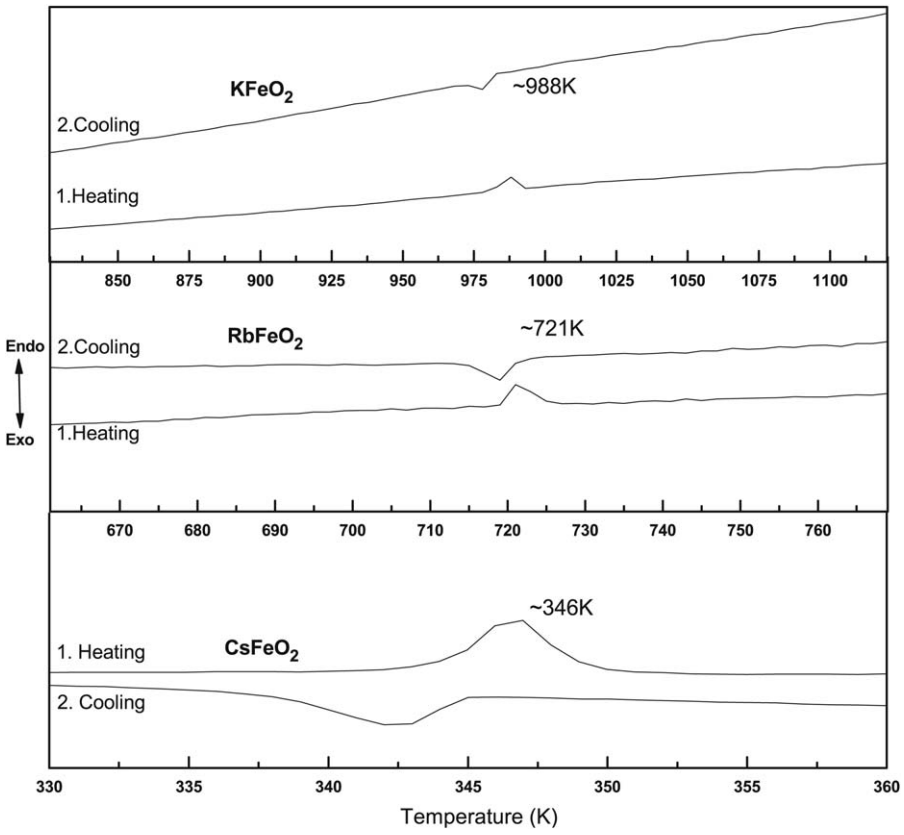

Fig. 3. Phase transitions detected by differential scanning calorimetry (DSC).

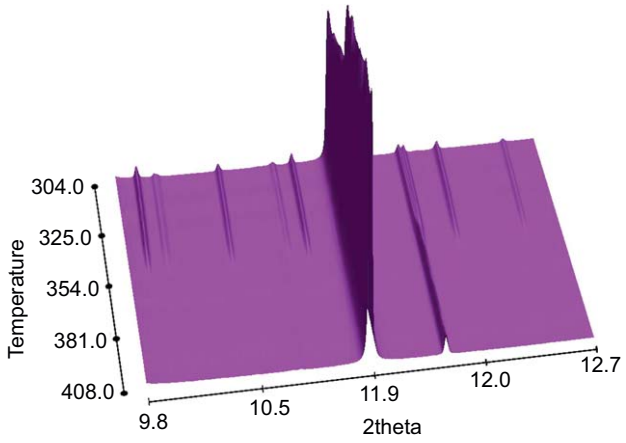

Fig. 4. Fragments (2θ range from 9.8° to 12.7°) of the synchrotron X-ray powder diffraction patterns of $CsFeO_2$ taken for this illustration with ~3 K steps on heating from 304 to 408 K.

In reasonable agreement with the DSC measurements, in synchrotron diffraction experiments some of the diffraction lines disappeared in $KFeO_2$ at ~1003 K, in $RbFeO_2$ at ~737 K, and in $CsFeO_2$ at ~350 K respectively, and the resulting high temperature phase could be indexed as cubic (space group $Fd\bar{3}m$).

The effect of this structural phase transition on the diffraction patterns is illustrated in Fig. 4 for the case of $CsFeO_2$. Qualitatively similar patterns have been recorded for $RbFeO_2$ and $KFeO_2$ showing phase transitions at ~737 K and ~1003 K respectively.

All the structural transformations are the first order displacive structural phase transition as can bee seen by volume discontinuity and appearance of abrupt disorder at the transition temperature. With the aid of high resolution synchrotron data, the precise monitoring of the structural parameters in the proximity of the phase transitions, alongwith the really tiny splitting of the diffraction lines due to the orthorhombic distortions can be seen.

3.2. Crystal structures of the low-temperature and high-temperature modifications

In agreement with the previously available results [46], the $KFeO_2$ crystal structure at room temperature has been found to possess the orthorhombic unit cell with lattice constants a=5.600 Å, b=11.25 Å, c=15.94 Å (thus $a \approx 1/2b \approx c/\sqrt{8}$), and the space symmetry *Pbca*. We find that at room temperature both $RbFeO_2$ and $CsFeO_2$ are isostructural to $KFeO_2$. The crystal structure parameters of all three compounds have been refined by synchrotron powder diffraction data for all temperatures. Tables 3 and 4 list the crystallographic data and atomic coordinates at the room temperature and at a temperature above the phase transition.

A perspective view of the orthorhombic low temperature structure is presented in Fig. 2, below. The Fe–O distances are very similar in all three structures and amount on average to 1.86 Å. However, when going from $KFeO_2$ to $RbFeO_2$ and to $CsFeO_2$, the unit cell volumes are increasing with the size of the alkali metal cation: from ~1003 Å^3 to ~1075 Å^3 to ~1179 Å^3. This gain of the volume in order to accommodate the alkali metal cations of corresponding bigger sizes is reflected by differences in the Fe–O–Fe bond angles: they grow at room temperature on average from 137° to 143° and 157° for $KFeO_2$, $RbFeO_2$ and $CsFeO_2$, respectively (Table 5). Thus, in the compound with the largest *A* cation (in $CsFeO_2$), the Fe–O–Fe connections are much more "straight" than in $RbFeO_2$ and in $KFeO_2$, where they are the most

Table 5
Bond angles Fe–O–Fe/° in the orthorhombic low temperature phases of $AFeO_2$ (A=K, Rb, Cs), describing the twisting of the FeO_4 tetrahedra.

Angle	$KFeO_2$ (Sync.) 298 K	$RbFeO_2$ (Sync.) 298 K	$CsFeO_2$ (Sync.) 298 K	$CsFeO_2$ (X-ray) 298 K	$CsFeO_2$ (X-ray) 100 K
Fe1–O1–Fe2	147.8(8)	152.8(1)	160.7(9)	156.3(6)	158.0(4)
Fe1–O2–Fe2	136.3(8)	141.5(1)	155.1(1)	152.2(5)	149.2(3)
Fe2–O3–Fe2	138.7(7)	146.5(1)	153.7(4)	158.5(4)	153.4(3)
Fe1–O4–Fe1	132.8(7)	140.9(1)	155.3(7)	161.6(4)	154.8(3)

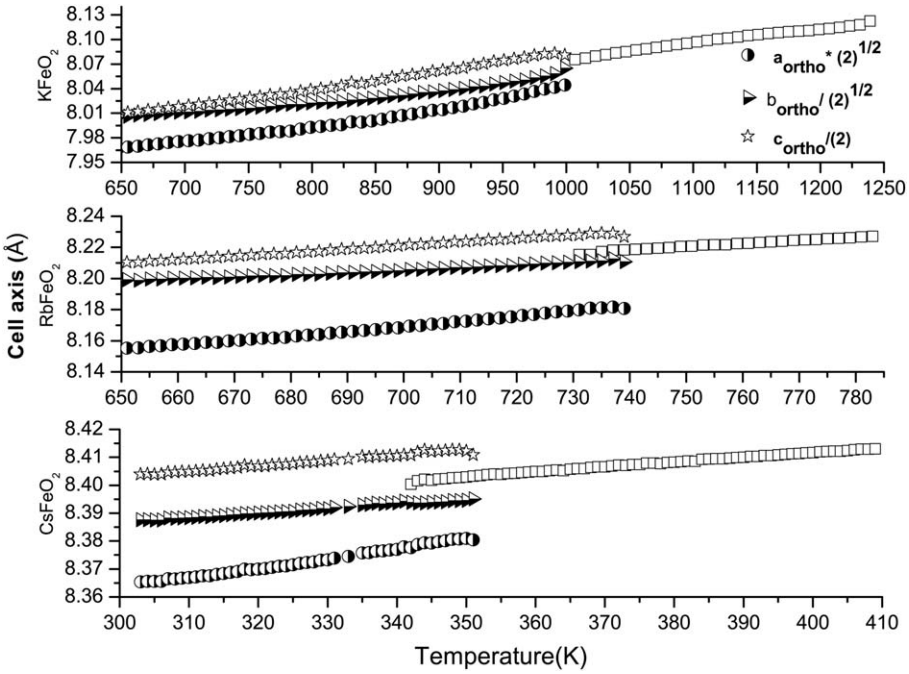

Fig. 5. Temperature dependence of unit cell parameters of $AFeO_2$ (A=K, Rb, Cs) as refined from the synchrotron data.

bent. Following as a result, the distances between nearest iron atoms are the smallest in $KFeO_2$ (3.45 Å on average), intermediate in $RbFeO_2$ (3.53 Å on average) and the largest in $CsFeO_2$ (3.63 Å on average).

The high temperature modifications of all three compounds (emerging at different temperatures) have been found to also be isostructural to each other. All the diffraction patterns of the high-temperature modifications of $KFeO_2$, $RbFeO_2$ and $CsFeO_2$ have been indexed on a cubic F-centered unit cell with a lattice constant a_{cub} related to those of the corresponding orthorhombic low-temperature modifications as: $a_{cub} \approx a_{orth} \cdot \sqrt{2} \approx b_{orth}/\sqrt{2} \approx 1/2 \cdot c_{orth}$. The structures have been determined to possess the $CsAlO_2$ type of structure (see Fig. 2, above), with the main structural parameters being tabulated in Tables 3 and 4.

The structural phase transitions in all three compounds are of the first order according to the results of DSC measurements and Rietveld refinements of the synchrotron X-ray data, the low-temperature orthorhombic and the high-temperature cubic phases are coexisting in certain temperature ranges, and abrupt changes in the lattice parameters and the unit cell volume can be seen clearly. This is illustrated in Fig. 4 for the case of $CsFeO_2$, and Fig. 5 shows the lattice parameters for all compounds as a function of temperature.

The temperature range of coexistence of the low-and high-temperature modifications of $CsFeO_2$ is ~12 K wide. A qualitatively similar situation has been observed in $RbFeO_2$, with the estimated width of the temperature range where the two phases are coexisting of ~8 K. The steps in temperature in the heating experiment of $KFeO_2$ were too coarse (8 K) to give an estimate for the same temperature range of the phase coexistence for $KFeO_2$, but the discontinuity of the lattice constants and unit cell volume at the transition from orthorhombic to cubic phase is qualitatively similar to the other two compounds (Fig. 5). The estimated transition temperatures (determined as those where the phases are in the 50:50 proportions) are thus ~1003, ~737 and ~350 K for $AFeO_2$, where A=K, Rb, Cs.

In case of $CsFeO_2$ because of the feasibility to achieve the transition temperature of 358 K, single crystal X-ray measurements were performed at 100, 298, and 400 K (cf. Tables 1 and 2). The measurements confirm the results obtained from powder diffraction data, in principle. The disappearance of some of the intensity peaks at 400 K is clearly visible (Fig. 1).

To a first approximation, the diffraction intensities of the investigated crystal of $CsFeO_2$ could be indexed and integrated on the basis of the cubic crystal system with a_{cubic}=16.784(2) Å at 298 K and 16.7123(2) at 100 K, respectively. This is an eightfold unit cell with doubled a-axis. The displacement parameters were found to be much too high, and no O-atoms could be localized in the difference-Fourier map.

It has turned out, however, that like for $RbFeO_2$ [29], the apparent cubic symmetry is an artifact caused by superposition of six, differently oriented domains, resulting in a reticular pseudo-merohedrally twinned crystal. The orientations of the six domains are represented by the polyhedron shown in Fig. 1, where each domain is shown in a different color. The twinning phenomenon is a result of the phase transition and thus a result of the synthesis procedure at high temperatures and the subsequent cooling to room temperature (transformation twin). With the complete data

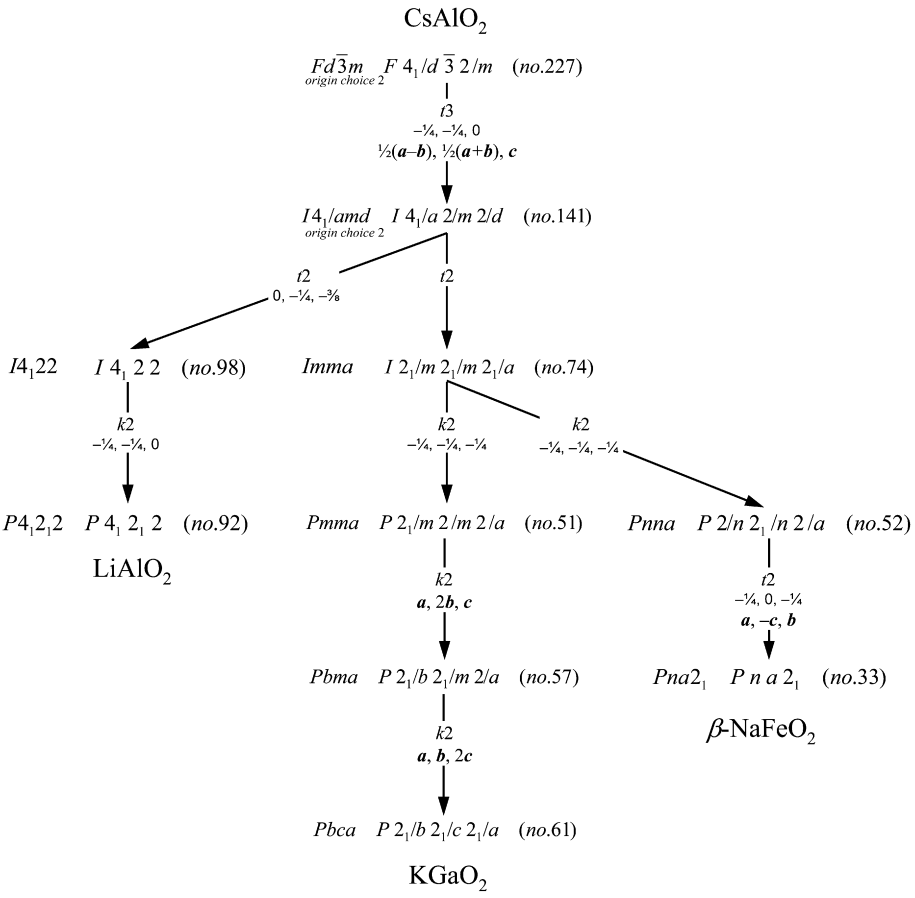

Fig. 6. Group–subgroup relation between $CsAlO_2$, $LiAlO_2$, $KGaO_2$, and β-$NaFeO_2$ (Bärnighausen-tree [47–49]).

set, including all six domains, it was possible to locate the O atoms via a difference-Fourier synthesis. All atoms were refined anisotropically and the resulting twin volume fractions showed reasonable values in the order of magnitude of 1/6 for all six domains.

A comparable twinning phenomenon is also observed for the structurally related high/low phase transition of cristobalite. Below 500 K the cubic high-temperature modification (β-cristobalite) transforms into the tetragonal low-temperature modification (α-cristobalite) with three or six different twin domains present [3,4].

The group–subgroup relation [47,48] between the aristotype $CsAlO_2$ and $KGaO_2$ includes two consecutive steps of symmetry reduction of the type translationengleich (*t*3 and *t*2, Fig. 6), which can be associated with multiple twinning in terms of "twins by twins", and resulting in six (3×2) twinning fractions, as observed. Fig. 6 shows the group–subgroup relation (*Bärnighausen-Stammbaum* [49]), including the entire site transformations, and the related structure types $LiAlO_2$ and β-$NaFeO_2$.

In Fig. 7, fragments of the crystal structures are shown on the example of $RbFeO_2$, below and above the phase transition, with the illustration of the strongly anisotropic character of the atomic thermal vibrations of the oxygen atoms at high temperatures (Fig. 7, top). These observations allow for tentative approach to rationalize the mechanism of phase transition. In fact, one may even think of the phase transition mechanism in such a way that as soon as with raising the temperature, increase in the atomic displacement parameters become large enough, the oxygen atoms "jump" from a given position with a well-defined Fe–O–Fe bond angle into a symmetrically related state illustrated in Fig. 7 (top) where these angles are of course also preserved. In time-average, all these equally possible orientations are observed in form of an apparently 180° Fe–O–Fe angle with unphysically-short Fe–O bond lengths and strongly anisotropic displacement parameters for the oxygen atoms. Reversely the bending angles lock in, when lowering the temperature, and due to the symmetry relations (Fig. 6), which is the origin of the observed twinning phenomenon, there are six possibilities of how this ordering can take place. Fig. 7 (below) shows, on the example of $RbFeO_2$, two of the six possible mutual orientations of the $^3_\infty[FeO_{4/2}]^-$ framework, with the displacement ellipsoids drawn for one of them, indicating a well ordered structure, but a twinned crystal.

4. Conclusion

All the three $AFeO_2$ (A=K, Rb and Cs) compounds were synthesized with the help of the azide nitrate route [32,33], whereupon the concomitant structures and phase transitions in the $AFeO_2$ (A=K, Rb, Cs) compounds were systematically investigated by high resolution synchrotron X-ray powder diffraction technique. The low-temperature and high-temperature modifications of all three compounds are isostructural to each other. The orthorhombic structure with *Pbca* space group is encountered at low temperature [46] and the cubic one with space symmetry $Fd\bar{3}m$ is the high temperature modification. Likewise in case of $CsFeO_2$ because of feasibility to achieve the transition temperature of 358 K using Brucker AXS single crystal diffractometer, the same transition was counter verified using single crystal data. Our findings differ distinctly from previously reported room temperature cubic ($Fd\bar{3}m$) structure of $CsFeO_2$ [30]. The insights obtained are expected to facilitate the understanding of the magnetic superexchange mechanisms and their dependencies on the

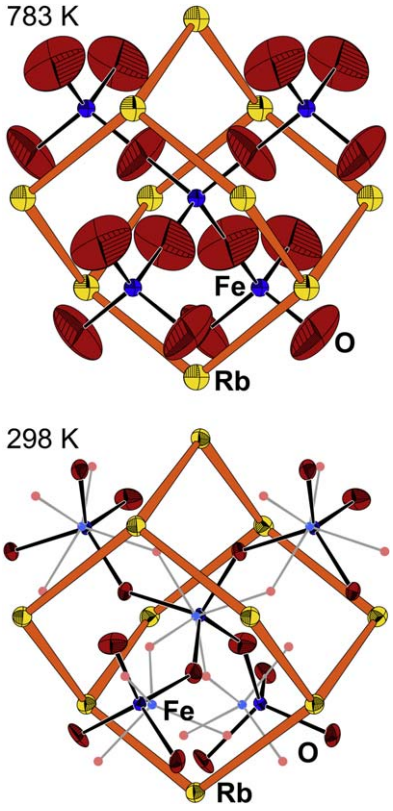

Fig. 7. Fragment of the $RbFeO_2$ structure. Top: cubic structure at 783 K. Below: orthorhombic structure at 298 K, with a second possible orientation of the FeO_4 tetrahedra drawn in smaller circles, they represent another twin domain on one hand, or the thermal motion of iron and oxygen at high temperature on the other hand. Displacement ellipsoids are drawn at the 50% probability level for both figures.

Fe–O–Fe angles and distances varying with temperature, in particular on the dynamic disorder of the unclear structure. While the temperatures of the displacive structural phase transitions differ significantly in the three studied compounds (~1003, ~737 and ~350 K for *A*=K, Rb, Cs), the magnetic transition temperatures are very close to each other and are discussed separately [50].

Acknowledgments

The Swiss Light Source Materials Science Beamline Powder Diffraction Station in Villigen is gratefully acknowledged for Synchrotron beam time. N.Z. Ali is indebted for the financial support from the Higher Education Commission (HEC) Pakistan and the German Academic Exchange Service (DAAD) in the form of a fellowship.

References

[1] T.F.W. Barth, Am. J. Sci. 24 (1932) 97–110.
[2] W. Nieuwenkamp, Z. Kristallogr. 92 (1935) 82–88.
[3] W.A. Dollase, Z. Kristallogr. 121 (1965) 369–377.
[4] D.R. Peacor, Z. Kristallogr. 138 (1973) 274–298.
[5] R.W.G. Wyckoff, Am. J. Sci. 9 (1925) 448–459.
[6] T.F.W. Barth, Am. J. Sci. 23 (1932) 350–356.
[7] W. Nieuwenkamp, Z. Kristallogr. 96 (1937) 454–458.
[8] A.J. Leadbetter, T.W. Smith, A.F. Wright, Nat. Phys. Sci. 244 (1973) 125–126.
[9] A.F. Wright, A.J. Leadbetter, Philos. Mag. 31 (1975) 1391–1401.
[10] M. O'Keefe, B.G. Hyde, Acta Crystallogr. B 32 (1976) 2923–2936.
[11] W.W. Schmahl, I.P. Swainson, M.T. Dove, A. Graeme-Barber, Z. Kristallogr. 201 (1992) 125–145.
[12] I.P. Swainson, M.T. Dove, D.C. Palmer, Phys. Chem. Miner. 30 (2003) 353–365.
[13] D.R. Spearing, I. Farnan, J.F. Stebbins, Phys. Chem. Miner. 19 (1992) 307–321.
[14] B.L. Phillips, J.G. Thompson, Y. Xiao, R.J. Kirkpatrick, Phys. Chem. Miner. 20 (1993) 341–352.
[15] A. Takada, P. Richet, C.R.A. Catlow, G.D. Price, J. Non-Cryst. Solids 354 (2008) 181–187.
[16] G.L. Hua, T.R. Welberry, R.L. Withers, J.G. Thompson, J. Appl. Crystallogr. 21 (1988) 458–465.
[17] L. Gracia, J. Contreras-Garcia, A. Beltran, J.M. Recio, High Pressure Res. 29 (2009) 93–96.
[18] S.L.G. Husheer, J.G. Thompson, A. Melnitchenko, J. Solid State Chem. 147 (1999) 624–630.
[19] F. Liu, S.H. Garolfalini, R.D. King-Smith, D. Vanderbilt, Phys. Rev. Lett. 70 (1993) 2750.
[20] I.P. Swainson, M.T. Dove, Phys. Rev. Lett. 71 (1993) 3610.
[21] D. Taylor, Miner. Mag. 48 (1984) 65–79.
[22] D.M. Hatch, S. Ghose, Phys. Chem. Miner. 17 (1991) 554–562.
[23] I.E. Grey, R.J. Hill, A.W. Hewat, Z. Kristallogr. 193 (1990) 51–69.
[24] J.C. Anderson, M. Schieber, J. Phys. Chem. Solids 25 (1964) 961–968.
[25] R. Famery, P. Bassoul, F. Queyroux, J. Solid State Chem. 61 (1986) 293–300.
[26] R. Hoppe, Angew. Chem. 77 (1965) 551;
R. Hoppe, Angew. Chem. Int. Ed. Engl. 4 (1965) 534–535.
[27] E. Vielhaber, R. Hoppe, Z. Anorg. Allg. Chem. 369 (1969) 14–32.
[28] C.W.F.T. Pistorius, G.F. de Vries, Z. Anorg. Allg. Chem. 395 (1973) 119–121.
[29] J. Nuss, N.Z. Ali, M. Jansen, Acta Crystallogr. B 63 (2007) 719–725.
[30] G. Frisch, C. Röhr, Z. Naturforsch. 59b (2004) 771–781.
[31] T.F.W. Barth, J. Chem. Phys. 3 (1935) 323–325.
[32] D. Trinschek, M. Jansen, Angew. Chem. 111 (1999) 234–235;
D. Trinschek, M. Jansen, Angew. Chem. Int. Ed. Engl. 38 (1999) 133–135.
[33] M. Sofin, E.-M. Peters, M. Jansen, Z. Anorg. Allg. Chem. 628 (2002) 2697–2700.
[34] H.D. Fair, R.F. Walker, Energetic Materials, Physics and Chemistry of Inorganic Azides, Plenium Press, New York and London, vol. 1. 1977, pp. 30–38.
[35] Bruker Suite, version 2008/3, Bruker AXS Inc., Madison, WI, USA, 2008.
[36] J. Nuss, M. Jansen, Acta Crystallogr. B 63 (2007) 843–849.
[37] G.M. Sheldrick, TWINABS–Bruker AXS scaling for twinned crystals, version 2008/4, University of Göttingen, Germany, 2008.
[38] G.M. Sheldrick, SADABS–Bruker AXS area detector scaling and absorption, Version 2008/1, University of Göttingen, Germany, 2008.
[39] G.M. Sheldrick, Acta Crystallogr. A 64 (2008) 112–122.
[40] G. Langlet, C.R. Hebd, Seances Acad. Sci. 259 (1964) 3769–3770.
[41] 〈http://sls.web.psi.ch/view.php/beamlines/ms/pd/index.html〉.
[42] M.E. Fleet, Acta Crystallogr. B 37 (1981) 917–920.
[43] S. Nariki, S. Ito, K. Kozawa, T. Uchida, N. Yoneda, Solid State Ionics 40–41 (1990) 95–98.
[44] A. Niwata, K. Itoh, J. Phy. Soc. Jpn. 64 (1995) 4733–4738.
[45] J. Rodríguez-Carvajal, Physica B 192 (1993) 55–69.
[46] Z. Tomkowicz, A. Szytuła, J. Phys. Chem. Solids 38 (1977) 1117–1123.
[47] H. Wondratschek, U. Müller (Eds.), International Tables for Crystallography, Vol. A1, Kluwer Academic Publishers, Dordrecht, The Netherlands, 2004.
[48] U. Müller, Z. Anorg. Allg. Chem. 630 (2004) 1519–1537.
[49] H. Bärnighausen, MATCH, Commun. Math. Chem. 9 (1980) 139–175.
[50] N.Z. Ali, D. Sheptyakov, M. Jansen, Paper in progress.